Membrane Hydrocarbon Thickness Modulates the Dynamics of a Membrane Transport Protein

Qi Xu, Miyeon Kim, K. W. David Ho, Pawel Lachowicz, Gail E. Fanucci, and David S. Cafiso
Department of Chemistry and Biophysics Program, University of Virginia, Charlottesville, Virginia 22904-4319

ABSTRACT Nitroxide spin labels were incorporated into selected sites within the β-barrel of the bacterial outer-membrane transport protein BtuB by site-directed mutagenesis, followed by chemical modification with a methanethiosufonate spin label. The electron paramagnetic resonance lineshapes of the spin-labeled side chain (R1) from these sites are highly variable, and have spectral parameters that reflect secondary structure and local steric constraints. In addition, these lineshape parameters correlate with crystallographic structure factors for Cα carbons, suggesting that the motion of the spin label is modulated by both the local modes of motion of the spin label and the local dynamics of the protein backbone. Experiments performed as a function of lipid composition and sample temperature indicate that nitroxide spin labels on the exterior surface of BtuB, which face the membrane hydrocarbon, are not strongly influenced by the phase state of the bulk lipids. However, these spectra are modulated by membrane hydrocarbon thickness. Specifically, the values of the scaled mobility parameter for the R1 lineshapes are inversely proportional to the hydrocarbon thickness. These data suggest that protein dynamics and structure in BtuB are directly coupled to membrane hydrophobic thickness.

INTRODUCTION

Membrane proteins experience a heterogeneous environment where interactions occur both with the aqueous phase and with membrane lipids. Not surprisingly, the activity of membrane proteins was found to be highly dependent on the lipid composition of the membrane (1). A number of properties of a bilayer, which are determined by lipid composition, are believed to influence membrane protein activity. For example, native biological membranes are often composed of lipids that tend to form nonbilayer phases. These lipids prefer to occupy a curved surface, and their presence in a flat lamellar phase introduces a strain into the bilayer (2,3). This strain was proposed to modulate membrane protein function (4,5). The electrostatic properties of the bilayer also vary as a function of lipid composition (6–9), and electrostatics is often a major driving force in binding proteins to bilayers. The reversible electrostatic association of many membrane-binding domains, such as the effector domain of the myristoylated alanine-rich C-kinase substrate (10), and the Ca^{2+}-dependent C2 domains, is critical for cell-signaling and membrane-trafficking (11). Finally, the thickness of the lipid bilayer is also dependent on lipid composition, and membrane proteins are thought to be adapted to membranes of a defined thickness. A hydrophobic mismatch exists when the thickness of the lipid bilayer does not match the hydrophobic surface of the protein (12).

Hydrophobic matching is a well-accepted concept (1), and there is good evidence that lipids in the bilayer can adopt a conformation to match the hydrophobic surface of a membrane protein, either by shortening or lengthening (13,14). In addition, hydrophobic matching and membrane thickness can affect the activity (15–17), orientation (18), stability (19), and aggregation state (20,21) of membrane proteins.

Although much has been learned from the studies listed above, the majority of work on protein-membrane interactions was performed on helical membrane proteins or model helical peptides. Membrane proteins based on helices are generally thought to be flexible so that they adapt and distort, by tilting in the bilayer or altering their packing, in response to changes in bilayer thickness or other bilayer properties. For example, the mechanosensitive channels gate in response to bilayer properties, and the helices of these proteins undergo a dramatic change in tilt in response to altered lipid composition (22). The effects of lipid composition on the structure or dynamics of β-barrel membrane proteins are not as well-characterized. These proteins are generally thought to be rigid because of the extensive hydrogen bonding network between the strands of the barrel. However, there are indications that such structures may couple to membrane thickness. For example, lipid-binding measurements suggest that the β-barrel from the *Escherichia coli* outer-membrane porin OmpF distorts in the presence of lipids longer than 20 carbons (23), and the thermal stability of the outer membrane porin OmpA to unfolding was found to be related directly to hydrocarbon thickness (19).

Submitted March 15, 2008, and accepted for publication June 5, 2008.

Address reprint requests to David S. Cafiso, Dept. of Chemistry, University of Virginia, Charlottesville, VA 22904-4319. Tel.: 434-924-3067; E-mail: cafiso@virginia.edu.

Qi Xu's present address is Epic Therapeutics, 220 Norwood Park South, Norwood, MA 02062.

Miyeon Kim's present address is the Jules Stein Eye Institute, University of California at Los Angeles School of Medicine, Los Angeles, CA 90095.

Gail E. Fanucci's present address is the Dept. of Chemistry, University of Florida, Gainesville, FL 32611.

Editor: David D. Thomas.

0006-3495/08/09/2849/10 $2.00

doi: 10.1529/biophysj.108.133629

Here, we present evidence that the dynamics and conformation of the outer-membrane vitamin B_{12} transport protein, BtuB, are coupled with lipid bilayer thickness. The outer-membrane vitamin B_{12} transport protein belongs to a family of membrane transport proteins that are termed ''TonB-dependent''. These membrane proteins function in the high-affinity uptake of rare nutrients, and they derive energy for transport by coupling to the inner-membrane protein TonB. There are a number of structures for this class of transporters, including BtuB (24), which are all based on a 22-stranded antiparallel β-barrel. Here, we make use of an electron paramagnetic resonance (EPR)-based methodology termed ''site-directed spin-labeling'' (25–27), and incorporate the spin-labeled side chain R1 (Fig. 1 *A*) into various sites within three different transmembrane β-strands of BtuB (Fig. 1 *B*).

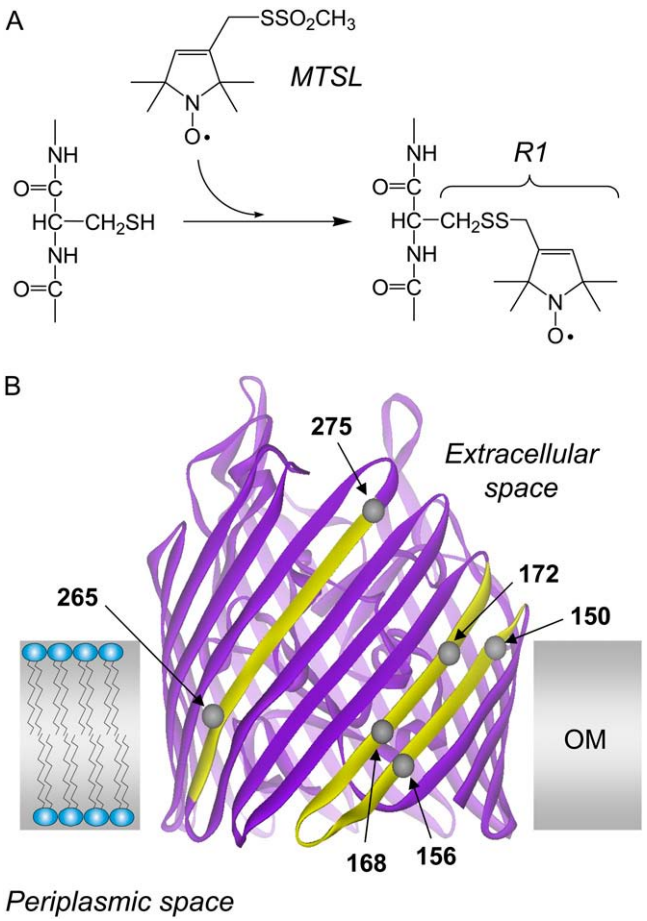

FIGURE 1 (*A*) R1 spin-label side chain is incorporated into proteins by derivatizing single cysteines with the MTSL. (*B*) Model of *Escherichia coli* vitamin B-12 transport protein BtuB (Protein Data Bank identification, 1NQE (24)). The BtuB is structurally homologous to other TonB-dependent transporters, and is based on a β-barrel consisting of 22 antiparallel β-strands, with an N-terminal core domain that fills the interior of the barrel (51). Shaded region indicates the approximate location of the membrane bilayer (33). The spin-labeled side chain, R1, has been incorporated into over 30 sites on β-strands 2, 3, and 7, which are highlighted. Several labeled sites are shown: residues 150 and 156 on strand 2, residues 168 and 172 on strand 3, and residues 265 and 275 on strand 7.

The results show that the EPR lineshapes obtained are influenced by interactions of the spin label with neighboring residues on adjacent β-strands in the BtuB barrel and the dynamics of the protein backbone (inferred from x-ray B-factors). Furthermore, spectral lineshapes are modulated by the lipid composition of the bilayer into which BtuB is reconstituted, and for hydrocarbon-facing sites in strand 2, a linear relationship exists between the membrane hydrocarbon thickness and the scaled mobility parameter obtained from the EPR spectrum. The data provide a strong indication that membrane thickness modulates the dynamics and structure of BtuB.

EXPERIMENTAL METHODS

Materials

The sulfhydryl-reactive spin-labeled methanethiosulfonate, *S*-(1-oxy-2,2,5,6-tetramethylpyrroline-3-methyl) methanethiosulfonate (MTSL), was purchased from Toronto Research Chemicals (Toronto, Ontario, Canada). The DL-dithiothreitol and cholesterol were from Sigma (St. Louis, MO), sarkosyl was from Fisher Chemical (Pittsburgh, PA), and phenylmethanesulfonyl fluoride was purchased from Boehringer Mannheim (Indianapolis, IN). The detergent *n*-octyl-β-*D*-glucopyranoside (OG), Anagrade, was purchased from Anatrace (Maumee, OH). The lipids 1-palmitoyl-2-oleoyl-*sn*-glycero-3-phosphocholine (POPC) (16:0, 18:1), 1,2-dimyristoyl-*sn*-glycero-3-phosphocholine (DMPC) (di-14:0), 1,2-dilauroyl-*sn*-glycero-3-phosphocholine (DLPC) (di-12:0), 1,2-dioleoyl-*sn*-glycero-3-phosphocholine (DOPC) (di-18:1), 1,2-dieicosenoyl-*sn*-glycero-3-phosphocholine (DiEiPC) (di-20:1), and 1,2-dierucoyl-*sn*-glycero-3-phosphocholine (DiErPC) (di-22:1) were purchased from Avanti Polar Lipids (Alabaster, AL).

Expression, labeling with MTSL, purification, and reconstitution of BtuB

The expression, labeling with MTSL, and purification of BtuB mutants were performed as previously described (28). The BtuB was then reconstituted by dialysis from mixed micelles of protein and lipid, as detailed elsewhere (28). Briefly, mixed micelles were prepared by drying the appropriate phosphatidylcholine in chloroform under a stream of N_2, followed by vacuum desiccation overnight to remove any residual solvent. The dried lipid was hydrated in a buffer containing 10 mM HEPES, 130 mM NaCl, pH 6.5, to which OG had been added at a lipid/detergent ratio of 1:4 (w/w). The lipid-detergent mixture was then incubated with purified BtuB for ~1 hr at room temperature, to yield mixed micelles at a lipid/protein ratio of 500:1 or higher. Reconstituted protein-lipid vesicles were obtained by removing the detergent from the mixed micelles, using 10 kDa MWCO Spectra/Por CE dialysis membranes (Spectrum Laboratories, Rancho Dominguez, CA). The dialysis buffer contained 10 mM HEPES, 130 mM NaCl, 0.25 mM NaN_3, and 1 μM EDTA, pH 6.5, and dialysis proceeded for 3 days with six 4-L buffer changes for reconstitution into POPC vesicles. The reconstituted vesicles were collected by centrifugation, and were further concentrated using a Beckman Airfuge (Beckman Coulter, Fullerton, CA). Residual levels of OG were low, and could not be detected by thin-layer chromatography in these reconstituted samples.

Electron paramagnetic resonance

The EPR spectroscopy was performed on a Varian E-line 102 series X-band spectrometer equipped with a loop-gap resonator (Medical Advances, Milwaukee, WI). Spectra were acquired and analyzed using LabView software

that was generously provided by Drs. Christian Altenbach and Wayne Hubbell (University of California, Los Angeles, CA). All spectra were recorded from samples prepared in glass capillary tubes with a 0.8-mm inner diameter. (VitroCom, Mountain Lakes, NJ), using 2.0 mW of incident microwave power and a 100-kHz modulation amplitude of 1.0 G. Unless otherwise indicated, all spectra were 100-G field sweeps. Temperature control was achieved using a Varian temperature controller, with a cavity Dewar designed to hold the loop gap resonator (Wilmad, Buena, NJ).

Several parameters can be measured easily from the nitroxide spectra that provide a qualitative measure of the motional averaging of the nitroxide. From the linewidth of the central nitroxide resonance, δ, a parameter termed the scaled mobility, M_s, can be determined using the expression:

$$M_s = \frac{(\delta^{-1} - \delta_i^{-1})}{(\delta_m^{-1} - \delta_i^{-1})},$$

where δ_m and δ_i represent the most mobile and immobile protein-associated linewidths observed, respectively (respective values of 1.8 and 8.5 G were used here), and M_s provides a relative measure of the rate of spin-label sidechain motion (where $M_s = 0$ represents the least mobile lineshapes seen in proteins, and $M_s = 1$ represents the most mobile lineshapes); M_s primarily reflects the rotational correlation time of the label, and it depends on the local structure surrounding the nitroxide, as well as the dynamics of the protein backbone on the nanosecond timescale (29–31). A second qualitative measure of label correlation time is the amplitude of the central nitroxide resonance (I_0) of an EPR spectrum that is normalized against the total number of spins (determined from the double integral of the first derivative spectrum). Narrower EPR spectra, which result from nitroxides with greater motional averaging, have greater values of I_0. Finally, the second moment of the EPR spectrum, which measures the overall width of the nitroxide EPR spectrum, is sensitive to both the correlation time and ordering of the nitroxide label. Second moments ($\langle H^2 \rangle$) were calculated using a LabView program (National Instruments, Austin, TX), provided by Dr. Christian Altenbach, that implements a second-moment calculation described previously (32). This spectral parameter includes both contributions from nitroxide rotational correlation time and ordering (31).

RESULTS

EPR spectra of hydrocarbon-facing nitroxides in BtuB are not affected by acyl chain order

The MTSL spin label was attached to single cysteine mutations that were prepared in the BtuB β-barrel. Outward-facing sites in the barrel were chosen, so that the spin-label faced the membrane hydrocarbon. To investigate the effects of acyl chain order on the EPR lineshapes of R1, a previously investigated site in strand 2, T156R1 (33), was used. Two labeled protein samples were prepared, where one was reconstituted into DMPC, and the other into POPC bilayers (see Experimental Methods). Shown in Fig. 2 are the resultant EPR spectra for these two samples as a function of temperature. The results are surprising. At $T = 17°C$, the spectra are nearly identical (Fig. 2, *A* and *B*). However, the thermotropic phase of these two membrane systems should be different, based on the transition temperature of each pure lipid component: DMPC (di-14:0) and POPC (16:0, 18:1) are in solid (gel) and fluid (liquid crystalline, Lα) phases, respectively. These results indicate that the R1 label motion is not affected by the order of the hydrocarbon acyl chains in the bulk lipid phase. It is interesting that as the temperature is increased, the spectra from T156R1 exhibit more motional averaging in membranes composed of DMPC than in membranes composed of POPC. As a result, the spectra for T156R1 when both samples are in the Lα phase at the same temperature are different. The lineshape from T156R1 when reconstituted into POPC is broader than that from DMPC, reflecting a larger degree of motional restriction in the nitroxide. The gel-to-Lα phase transition is accompanied by both an increase in the molecular disorder of the acyl chains and a thinning of the bilayer. One explanation for the observed lineshape changes is that the spin label is responding to changes in hydrocarbon thickness, as discussed below.

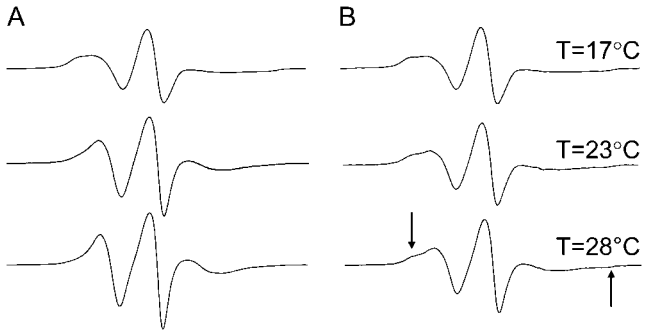

FIGURE 2 EPR spectra obtained at the X-band for the outward-facing spin-labeled BtuB mutant T156R1 in (*A*) DMPC and (*B*) POPC at three different temperatures (17°C, 23°C, and 28°C) extending below and above the gel-liquid crystalline phase transition of DMPC (23°C). (*B*) Arrows indicate positions of hyperfine extrema (2Azz′) for an immobilized component in the POPC spectrum of T156R1. T, temperature.

This effect was also observed for other spin-labeled sites in the BtuB β-barrel. Shown in Fig. 3 *A* is a series of superimposed EPR spectra at four positions along β-strand 2 at 17°C in both DMPC and POPC. For a given lipid system, the

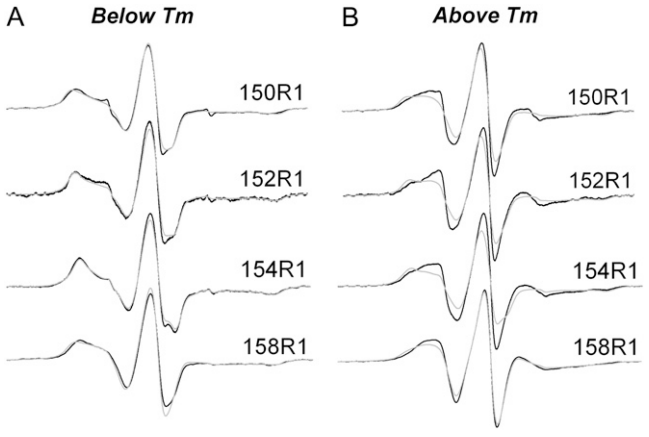

FIGURE 3 EPR spectra for the R1 spin label at hydrocarbon-facing sites 150, 152, 154, and 158 in β-strand 2 of the BtuB barrel reconstituted into POPC (*gray trace*) and DMPC (*black trace*), (*A*) below (17°C) and (*B*) above (28°C) the phase-transition temperature of DMPC. At each site, the spectra are virtually identical in either DMPC or POPC at 17°C, but differ at 28°C. The spectra indicate that R1 experiences more averaging in DMPC than in POPC in the liquid crystalline phase.

spectra at different positions along the strand vary, indicating that the spin-label motion is affected by protein structure. However, at this temperature, the spectra are nearly identical for a given site when the protein is reconstituted into DMPC and POPC lipids, again demonstrating that the spin-label motion is not altered by the ordering of the lipid bilayer acyl chains. However, when the temperature is raised to 28°C, i.e., a condition where both DMPC and POPC adopt the Lα phase, the EPR spectra for a given site are now different for the two lipid systems (Fig. 3 *B*). At every position, the spectra indicate that the R1 spin label undergoes more motional averaging on the nanosecond timescale when BtuB is reconstituted into DMPC than when reconstituted into POPC.

R1 motion in the BtuB barrel is correlated with membrane hydrocarbon thickness

To characterize further the effect that hydrocarbon thickness has on spin-label motion, spin-labeled BtuB samples (T156R1) were reconstituted into four other lipid matrices: DLPC (di-12:0), DOPC (di-18:1), DiEiPC (di-20:1), and DiErPC (di-22:1). Shown in Fig. 4 are spectra obtained from T156R1, all at 23°C, reconstituted into four synthetic lipids of increasing chain length. At this temperature, all these lipids are in the Lα phase. As lipid thickness increases, the spectra broaden, indicating that nitroxide motion on the nanosecond timescale decreases as the chain length of the lipid increases. Spectral lineshapes can be compared in a semiquantitative manner with the lineshape parameters of normalized central intensity (I_0) and the second moment ($\langle H^2 \rangle$). Both of these quantities provide a qualitative measure of nitroxide motion (see Experimental Methods). Fig. 5 shows plots of the values of I_0 and the second moment for the T156R1 lineshape as a function of hydrocarbon thickness determined by x-ray scattering for these lipids in the Lα phase (34,35). These plots show a strong linear correlation between the motion of the R1 side chain on the barrel and the thickness of the bilayer hydrocarbon, and over the range of lipid chain lengths examined. A linear correlation is also evident for the scaled mobility, M_s, with an ~3-fold difference in the value of M_s over this range. As discussed below, the dependence of EPR spectra on hydrocarbon thickness does not reflect protein aggregation. The simplest explanation for the correlation shown in Fig. 5 is that the shape or dynamics of the BtuB barrel change with membrane hydrocarbon thickness. Next, we provide evidence that BtuB barrel structure and dynamics modulate the EPR lineshapes of R1 labeled barrel sites.

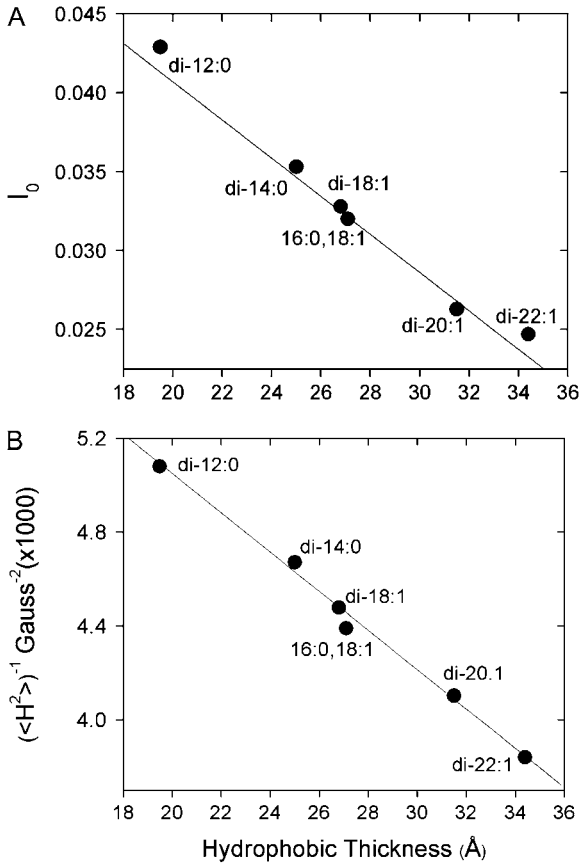

FIGURE 5 Plots of (*A*) normalized amplitude, I_0, and (*B*) second moment, $\langle H^2 \rangle$, obtained from EPR spectrum T156R1 reconstituted into different lipids as a function of lipid membrane hydrocarbon thickness. Data for lipid hydrocarbon thickness in the liquid crystalline phase were taken from previously published x-ray scattering data: DLPC and DiEiPC were from (34), and all other data were from (35). Errors in values of I_0 and $\langle H^2 \rangle$ are ~5%.

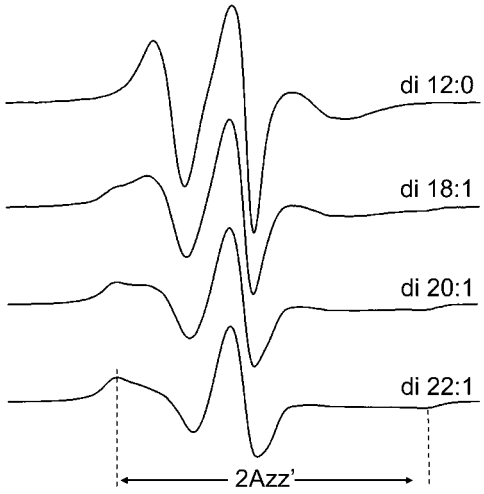

FIGURE 4 Comparison of EPR spectra for T156R1 at 23°C when the protein is reconstituted into four lipids of increasing chain length: DLPC (12:0), DOPC (18:1), DiEiPC (20:1), and DiErPC (22:1). As this lipid bilayer thickens, 159R1 becomes more immobile, as indicated by the increase in intensity of the immobilized component.

The R1 nitroxide in BtuB β-barrel interacts with residues in neighboring strands

Two outward-facing reporter sites, T267R1 and Y269R1, were chosen to investigate how the R1 label interacts with its

nearest neighbors. These sites were chosen because the hydrogen-bonded (HB) neighbors include a small amino-acid side chain (Ala for T267) and large amino-acid side chain (Trp for Y269). Mutations were made that switched the HB neighbor side chain for both sites, to alter the size and steric bulk of the neighbor. Fig. 6, *A* and *C*, show the EPR spectra for these reporter sites in the wild-type BtuB structure (T267R1/A252 and Y269R1/W250). The EPR lineshape for T267R1 contains two distinct spectral features in the low-field line, where the broader component (labeled *a*) reflects a more restricted motional mode and the narrower feature (labeled *b*) represents a more mobile motional mode of the spin label. These multicomponent lineshapes were seen in both T4 lysozyme and cellular retinoic binding protein, and were attributed to different configurations or rotameric states of the R1 side chain (36,37). The EPR spectrum of Y267R1, where the HB alanine neighbor is replaced by tryptophan (Y269R1/A252W), is shown in Fig. 6 *B*. The presence of the tryptophan side chain reduces the more mobile component (labeled *b*) of the EPR spectrum compared with that of T267R1/A252W, indicating that the R1 label exhibits more restricted motion in the presence of the larger neighbor. The spectrum of Y296R1 is shown in Fig. 6 *C*. This spectrum also results from an R1 side chain that has more than one motional mode, but in this case, R1 is highly restricted in its motion (the intensity of the *a* component is greater than the *b* component). The effect of substituting alanine for trytophan at the HB neighbor to position 296 is shown in Fig. 6 *D* (Y296R1/W250A). For Y269R1, switching the bulkier tryptophan for the smaller alanine side chain dramatically enhances the intensity of the more mobile component (labeled *b*) in the EPR spectrum of Y269R1/W250A, indicating that the label is less constrained when the neighboring residue is reduced in size. These data indicate that steric interactions with neighboring side chains modulate the lineshapes of spectra from spin labels incorporated into the β-barrel of BtuB, as they do in soluble β-sheet proteins (36).

The EPR spectra of R1 are influenced by local structure and curvature of the BtuB barrel

A series of 33 single cysteine mutations in strands 2, 3, and 7 of the barrel domain of BtuB was generated for site-directed spin-labeling studies with R1. Twenty representative EPR spectra from these sites are shown in Fig. 7. Fig. 7, *A* and *C*, show spectra from outward-facing sites on strands 7 and 3, respectively. Fig. 7 *B* shows spectra for sites in strands 2 and 3 that face into the barrel interior. The spectra from strands 2 and 3 were described previously (33), but were not interpreted in the context of the BtuB model obtained by x-ray crystallography (24). The spectral lineshapes of these labels are highly variable, reflecting significant differences in ni-

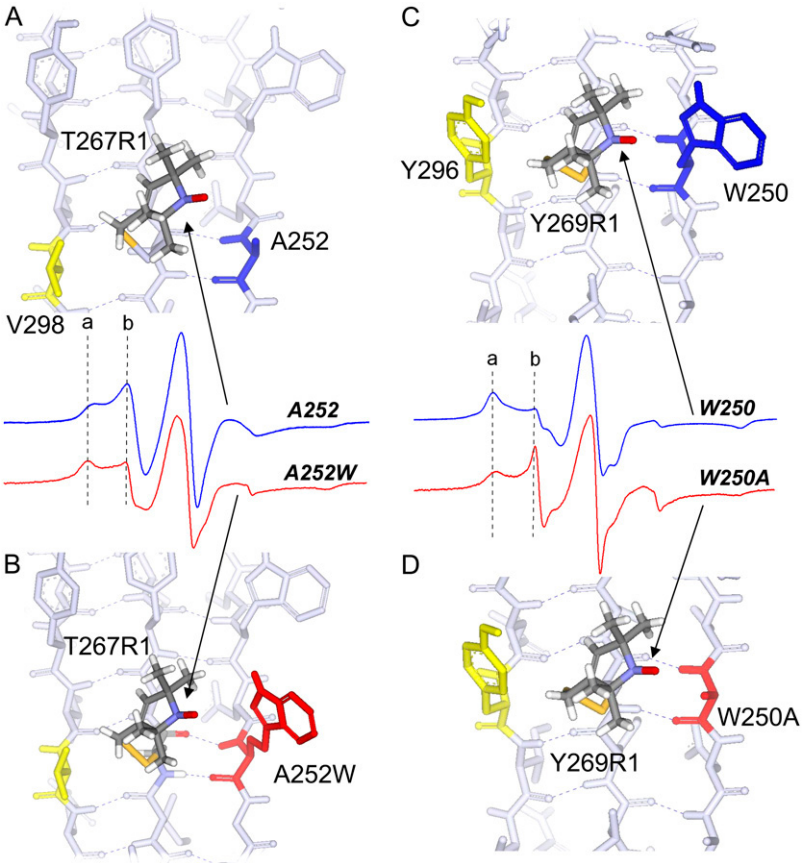

FIGURE 6 (*A*) Structure and EPR spectrum (*blue*) of T267R1 with wild-type HB and nonhydrogen-bonded neighbors A252 and V298 (in *blue* and *yellow*), respectively. (*B*) Structure and EPR spectrum (*red*) of T267R1 with HB neighbor mutated to tryptophan (A252W, in *red*). (*C*) Structure and EPR spectrum (*blue*) of T269R1 with wild-type HB and nonhydrogen-bonded neighbors W250 and Y296 (*blue* and *yellow*), respectively. (*D*) Structure and EPR spectrum (*red*) of T269R1 with HB neighbor mutated to alanine (W250A in *red*). Structures are based on the apo BtuB crystal structure (Protein Data Bank identification, 1NQE), with the spin-labeled side chain, R1, substituted as shown. The first R1 side-chain dihedral angles, χ_1 and χ_2, were set in the $\{m,m\}$ rotameric state (37). Dashed vertical lines *a* and *b* result from immobile and mobile motional modes in the R1 side chain, respectively.

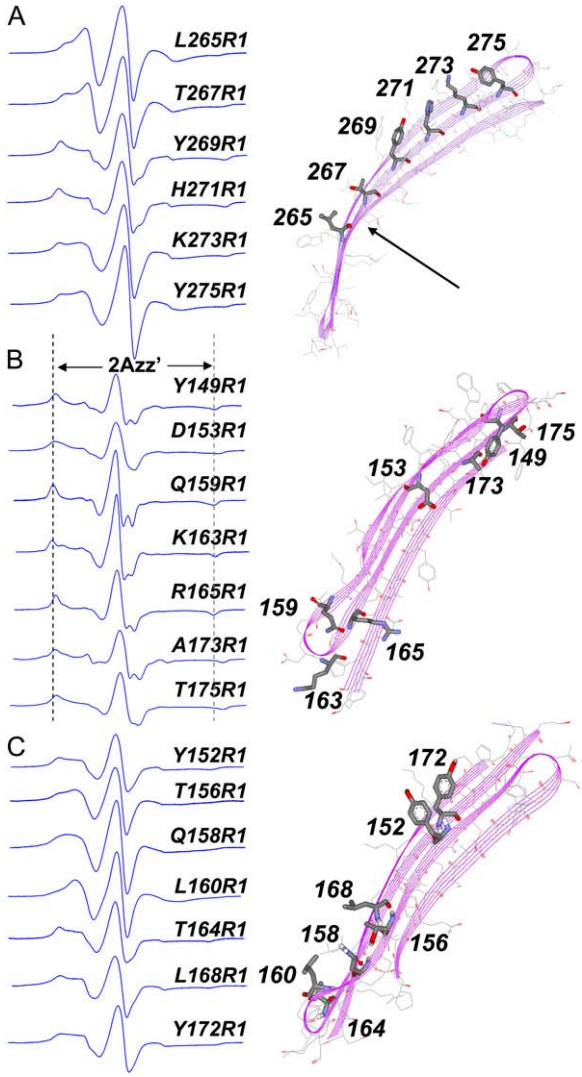

FIGURE 7 EPR spectra of R1 side chain incorporated into (*A*) outward-facing sites on strand 7, where arrow indicates a region on strand 7 with a highly positive (outward) curvature, (*B*) inward-facing sites on strands 2 and 3, and (*C*) outward facing sites on strands 2 and 3. Spectra *B* and *C* were previously described (33). Spin-labeled BtuB mutants were purified and reconstituted into POPC vesicles. (*B*) Labeled sites along strand 7.

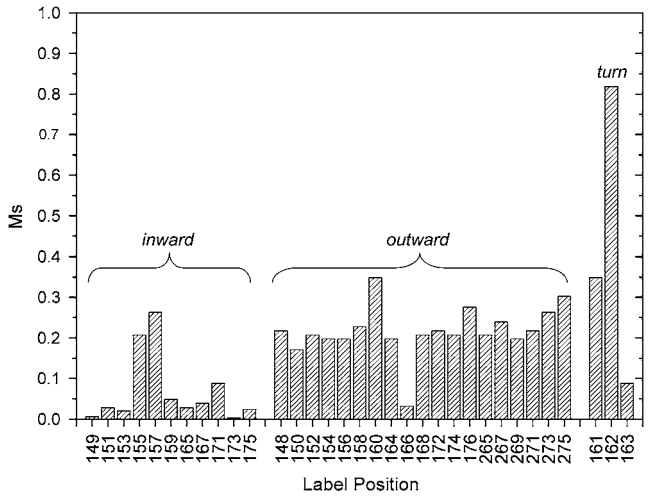

FIGURE 8 Scaled mobilities (M_s) for 33 spin-labeled sites in BtuB, calculated as described in Experimental Methods. The plot shows values of M_s that were obtained for spin labels that are positioned on the inward-facing and outward-facing surfaces of the BtuB barrel, and in the periplasmic turn that links the second and third barrel β-strands.

troxide motion among the various sites within the protein. For each of these sites, the scaled mobility, M_s, was determined from the central resonance linewidth, and is shown in Fig. 8.

The spectra obtained from inward-facing sites (Fig. 7 *B*) result from nitroxides that are highly constrained, with well-resolved hyperfine extrema (2Azz′) and correlation times >20 ns. This is generally true of the inward-facing sites examined, and the scaled mobilities for these sites (Fig. 8) are quite low. Inward-facing labels that are in tertiary contact with the hatch should yield highly immobilized spectra. However, a number of spectra in Fig. 7 *B* are immobilized, but are not in tertiary contact with the interior fold (e.g., positions 149, 159, and 173). This suggests that other factors, such as strong interactions with neighboring residues, are slowing the label motion. On the inward-facing surface of the barrel, interactions with neighboring residues are expected to be more pronounced because of the negative curvature of the surface. Labels at positions 155 and 157 exhibit a greater scaled mobility than other inward-facing residues, perhaps because they do not contact the N-terminal (hatch) region of BtuB, and are near the bend in strand 1 that connects the N-terminal hatch region with the barrel.

In comparison, labels placed at outward-facing sites, on the positively curved surface of the BtuB barrel, generally yield spectra (Fig. 7, *A* and *C*) of higher mobility than those on the inner surface (Fig. 8). The label at position 160 (Fig. 7 *C*) yields one of the more magnetically averaged spectra among this group ($M_s \sim 0.4$), probably because it is located at a site where the strand is only hydrogen-bonded to one neighboring strand. The fractional solvent-accessible surface area for L160 is quite high (0.59), and the R1 label at this site does not strongly interact with neighboring side chains. The short segments or turns linking the strands on the periplasmic surface of BtuB would be expected to yield the most mobile spectra, and this is indeed the case (the label at position 162 has a value of M_s near 0.8).

This difference between inward-facing and outward-facing spectra suggests that the curvature of the BtuB barrel influences R1 lineshape. Evidence for this effect is also seen in the spectra from strand 7 (Fig. 7 *A*). Two labels in this strand, 256R1 and 267R1, yield spectra that are more motionally averaged than those on the remainder of the strand (the second moments for these spectra are the lowest among those in Fig. 7 *A*). These side chains are positioned on a portion of strand 7 with a particularly high positive curvature (Fig. 7 *A*,

arrow), and the fractional solvent-accessible surface areas for the native side chains (0.42 in each case) are significantly higher than for other side chains in this group. These qualitative correlations indicate that the motion of the R1 label, when incorporated into BtuB, is dependent on barrel curvature, and this is physically reasonable. As discussed above, the R1 label interacts strongly with neighboring side chains in a β-sheet. As a result, the curvature of the sheet should modulate the nitroxide lineshape by modulating steric contact with neighboring residues.

R1 motion in the BtuB barrel is influenced by backbone dynamics

A comparison of EPR data with crystallographic data for BtuB provide an indication that the EPR lineshapes of R1 are sensitive to protein dynamics. Shown in Fig. 9 *A* are plots of the normalized intensity of the EPR central resonance (I_0) from spin-label sites along strands 2 and 3. The normalized intensity of the EPR spectrum provides a qualitative measure of the rate of motion of the R1 side chain, and there is a clear $i,i+2$ pattern in the values of I_0, consistent with the β-sheet configuration of the strands. In addition, the motional averaging of the R1 label increases as it is positioned closer to the periplasmic surface of the protein. Fig. 9 *B* shows a plot of the B-factors for the α-carbons determined by x-ray crystallography (24). The increasing B-factor toward the periplasmic surface parallels the normalized intensity observed in the EPR spectra. Although B-factors represent a combination of static and dynamic disorder, they are generally thought to reflect protein dynamics, and this correlation suggests that the increased nitroxide motion toward the periplasmic face of BtuB is a result of backbone dynamics. This conclusion is consistent with previous observations of water-soluble proteins, showing that the EPR spectrum of the R1 label is modulated by backbone dynamics (29–31).

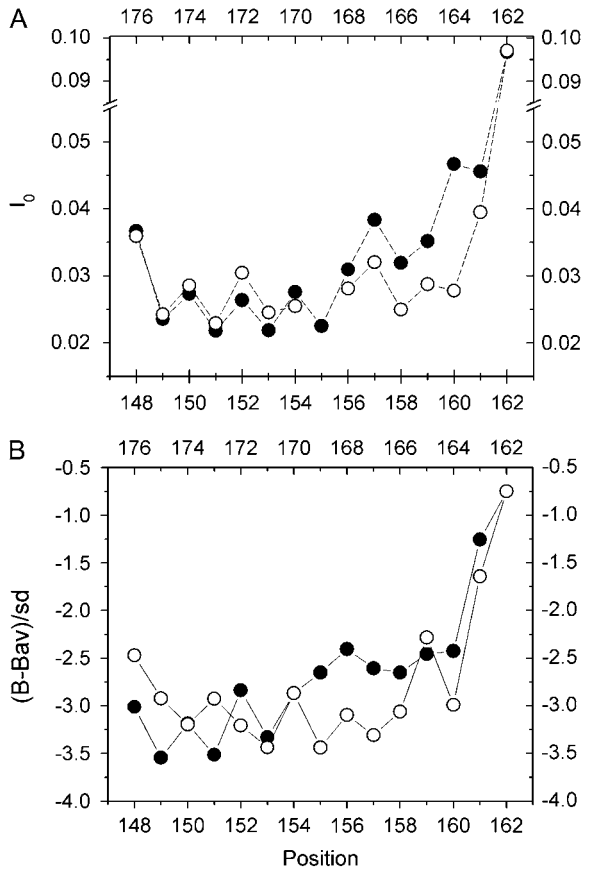

FIGURE 9 Comparison of (*A*) normalized amplitudes obtained by EPR spectroscopy for spin labels on strands 2 and 3 with (*B*) B-factors for the Cα carbons along strands 2 and 3. Structure factors are plotted as the difference from the average B-factor divided by the standard deviation (24). Solid circles represent data for strand 2 (residues 148–162), and open circles represent data for strand 3 (residues 162–176). Residues on the periplasmic surface of the transporter are on the right side of plots. (*A*) Data shown were published previously (33).

DISCUSSION

Site-directed spin labeling is a technique that combines site-directed mutagenesis with chemical labeling to incorporate nitroxides, such as the R1 side chain, at specific positions within a biomolecule. These EPR lineshapes are thought to reflect local protein structure, tertiary contact of the label, and nanosecond time-scale protein backbone dynamics (30,38). The data presented here are consistent with this previous work, and demonstrate that EPR lineshapes obtained from a spin-labeled transmembrane β-barrel also reflect local structure and dynamics, including the composition of neighboring side chains on adjacent β-strands and the curvature of the β-barrel. The unexpected finding (Figs. 2–5) is that the R1 lineshapes of spin labels within the BtuB β-barrel are sensitive to hydrocarbon thickness, and exhibit an increase in motional averaging as the membrane hydrocarbon thins.

Hydrocarbon thickness might modulate the EPR lineshape of the R1 label via several mechanisms. First, the labels might be responding directly to hydrocarbon chain order. However, as shown in Figs. 2 and 3, hydrocarbon-facing spin labels are not sensitive to the phase of the bulk lipid. Furthermore, the mobility of the R1 label seen in Fig. 9 increases as the labeled position is moved closer to the lipid interface. This is opposite to the direction of the acyl chain order profile in the lipid bilayer, which is well-known to decrease as one moves toward the interface (39). Second, it is possible that lipid composition modulates the aggregation state of the protein in this reconstituted system, and that the broader lineshapes seen when spin-labeled BtuB in POPC is compared with DMPC are the result of increased aggregation in POPC. However, there is no evidence for restricted accessibility of molecular oxygen or Ni(II) acetylacetonate to spin-labeled sites along strand 2 in POPC (33). Furthermore, fluorescence resonance energy transfer measurements (between BtuB mutants labeled with either a fluorescent donor or acceptor which are mixed and reconstituted) show no evidence for

different levels of aggregation of BtuB when incorporated into DMPC versus POPC (Q. Xu and D. S. Cafiso, unpublished data). Similarly, the extent and rate of intermolecular disulfide cross linking, which can be observed when single cysteines are incorporated into the flexible N-terminal region of BtuB (40), is similar when DMPC and POPC samples are compared (K. W. D. Ho and D. S. Cafiso, unpublished data). A third and likely source of the dependence of lineshape on membrane lipid composition is a direct coupling of protein structure or protein backbone dynamics with membrane lipid thickness.

How can changes in protein shape alter the EPR spectrum of the R1 label? As illustrated in Fig. 6, the EPR spectrum of the R1 side chain in BtuB is influenced by side-chain contact. Conceivably, changes in the shape of the barrel, because of changes in membrane hydrocarbon thickness, could alter the EPR spectra of the R1 label by changing the position of the neighboring side chains and the steric interference around the spin label. Changes in shape might also directly modulate the dynamics of barrel strands by restraining the geometry of β-strands. The data shown in Fig. 9 provide a strong indication that the EPR spectra from R1 in strands 2 and 3 may be modulated by the dynamics in the BtuB β-barrel. In addition to contributing directly to the motion of the spin label, backbone dynamics may modulate steric interactions of the R1 label with neighboring residue side chains, thereby modulating the energetics of interconversion between rotameric states of the label, and enhancing the motional averaging of the label.

Membrane proteins based on helical structures are generally thought to be quite flexible, and in a number of cases these proteins were shown to adapt as a function of membrane composition. For simple single-pass helical proteins, bilayer thickness was shown to modulate the tilt angle of the helix, presumably because tilt maintains the best match between the protein surface and bilayer thickness (41). Membrane thickness also appears to modulate the length of an unstructured region in the bacteriophage M13 coat protein (42). In visual rhodopsin, EPR spectroscopy indicated that the conformation of the protein in its bleached state is dependent on lipid thickness (43). Mechanosensitive channels gate as a result of membrane deformation because of curvature strain or thickness changes, and recent crystallographic and spectroscopic data indicate that gating involves a significant change in the tilt of transmembrane helices (22,44). In comparison, the conformational flexibility and adaptability of membrane proteins based on β-barrels are largely unexplored. Unlike helical proteins, membrane β-barrels are expected to be more rigid because of the extensive hydrogen-bonding network that cross-links the strands in the barrel. Nonetheless, the data presented here suggest that these β-barrel proteins have a degree of flexibility, and adapt to changes in membrane thickness. Thermodynamic data support such a conclusion. For the small, eight-stranded β-barrel protein, OmpA, thermal stability was shown to increase with hydrocarbon thickness (19), indicating that the protein structure is influenced by the thickness of the membrane hydrocarbon.

A number of mechanisms could be acting to couple hydrocarbon thickness with protein barrel dynamics in BtuB. Different lipid thicknesses are associated with different degrees of curvature strain or lateral pressure within the bilayer (3,4,45), and curvature strain or lateral pressure may act directly on the protein to alter is structure and dynamics. Conceivably, changes in membrane thickness may modulate the permeability or accessibility of water to the protein-membrane interface, thereby altering the exchange between water and interstrand hydrogen bonds. Another plausible model, given the structure of BtuB, involves a change in protein shape or dynamics in response to a hydrophobic mismatch. As the lipid thickness is altered, a mismatch between the hydrophobic protein surface and the membrane is likely to develop, leading to an energetically less favorable protein-membrane interaction. Although the lipids themselves are likely to change shape and alter the way they pack into the bilayer with a hydrophobic mismatch (23), the protein may also change shape to minimize this mismatch. Conceivably, the tilt of the strands within the β-barrel might change, either to lengthen or to compress the protein under the influence of the surrounding lipid. Such changes in shape should affect barrel curvature, modulate side-chain contact, and alter the dynamics of barrel strands.

The existence of a hydrophobic mismatch in many of the lipids used here seems likely when the locations of aromatic residues in BtuB that define the membrane interfacial region are examined. Shown in Fig. 10 is the crystal structure of BtuB, where the exterior-facing tryptophan and tyrosine residues near the membrane are highlighted. These residues are thought to define the interfacial region of the bilayer, and to reside in the vicinity of the glycerol group in the lipid bilayer (46). Also shown in Fig. 10 are boundaries defining the phosphate-to-phosphate thickness of DMPC and POPC bilayers obtained by x-ray diffraction (34). In contrast to the POPC bilayer, DMPC appears to fit the hydrophobic interface of BtuB. This is not unexpected. The lipopolysaccharide which makes up the outer leaflet of the *Escherichia coli* outer membrane has a complex polysaccharide structure, with multiple acyl chains averaging 14 carbons in length (47). If the BtuB barrel is flexible, it will adapt to increased hydrocarbon thickness by lengthening in a direction parallel to the bilayer normal, as shown in Fig. 10, *B* and *C*, thereby reducing the tilt of the β-strands and constraining motion in the strands. The changes seen in the EPR spectra of T156R1 with hydrocarbon thickness (Fig. 5) are consistent with decreased backbone dynamics in barrel strands, and we are presently testing the possibility that the observed changes in protein dynamics are driven by a change in protein shape.

What are the biological roles, if any, for these dynamic modes in the β-barrel of TonB-dependent transporters? Motion in the barrel may play a role in transport, by enabling interactions with TonB or by promoting the movement of the ligand through the barrel. Because there is no obvious path-

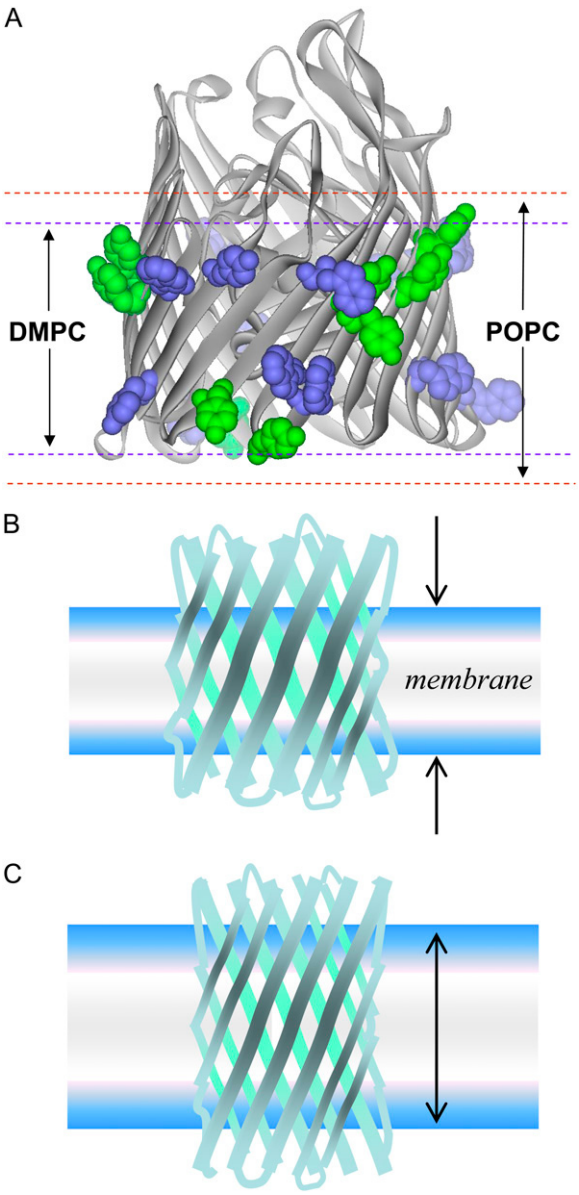

FIGURE 10 (*A*) Apo structure for BtuB (Protein Data Bank identification, 1NOE) shows external-facing tyrosine (*green*) and tryptophan (*blue*) residues within the bilayer in a space-filling rendering. Also shown (*dashed lines*) are approximate dimensions of phosphate-to-phosphate spacing of both a DMPC and a POPC bilayer. (*B* and *C*) A mechanism that could account for change in protein dynamics with lipid thickness. Altering the lipid thickness leads to a hydrophobic mismatch. Both the lipid and the protein respond to this mismatch. The protein responds by changing its length to accommodate the mismatch, leading to a change in orientation of the strands in the barrel.

way for substrate transport in high-resolution models of these transporters (48), it was proposed that structural rearrangements of the N-terminal region within the barrel are essential to transport (49). These structural changes might be quite extensive (50), and changes in shape of the barrel may help facilitate structural rearrangements by altering interactions between the N-terminus and the barrel. However, there is no information on the effect of lipid composition on the activity of any TonB-dependent transport protein, because this multiple-protein, two-membrane transport system has not been reconstituted.

In conclusion, the data presented here indicate that spin labels within the β-barrel of the outer-membrane transport protein BtuB yield EPR spectra that are sensitive to the local structure and backbone dynamics at the labeled site. The dynamics of these spin labels are also modulated by the thickness of the lipid bilayer into which the protein is reconstituted. This dependence on thickness most likely arises from the changes in protein shape and dynamics that accompany a hydrophobic mismatch.

We thank Drs. Robert Nakamoto and Linda Columbus for helpful discussions. Programs to analyze the continuous-wave EPR spectra shown here were generously provided by Drs. Wayne Hubbell and Christian Altenbach (University of California, Los Angeles).

This work was supported by grant GM 035215 from the National Institute of General Medical Sciences, National Institutes of Health.

REFERENCES

1. Jensen, M. O., and O. G. Mouritsen. 2004. Lipids do influence protein function—the hydrophobic matching hypothesis revisited. *Biochim. Biophys. Acta.* 1666:205–226.
2. Gruner, S. M. 1985. Intrinsic curvature hypothesis for biomembrane lipid composition: a role for nonbilayer lipids. *Proc. Natl. Acad. Sci. USA.* 82:3665–3669.
3. Gruner, S. M. 1989. Stability of lyotropic phases with curved interfaces. *J. Phys. Chem.* 93:7562–7570.
4. Cantor, R. S. 1999. Lipid composition and the lateral pressure profile in bilayers. *Biophys. J.* 76:2625–2639.
5. van den Brink-van der Laan, E., J. A. Killian, and B. de Kruijff. 2004. Nonbilayer lipids affect peripheral and integral membrane proteins via changes in the lateral pressure profile. *Biochim. Biophys. Acta.* 1666: 275–288.
6. McLaughlin, S. 1977. Electrostatic potentials at membrane-solution interfaces. *Curr. Top. Membr. Transp.* 9:71–144.
7. McLaughlin, S. 1989. The electrostatic properties of membranes. *Annu. Rev. Biophys. Biophys. Chem.* 18:113–136.
8. Franklin, J. C., D. S. Cafiso, R. F. Flewelling, and W. L. Hubbell. 1993. Probes of membrane electrostatics: synthesis and voltage-dependent partitioning of negative hydrophobic ion spin labels in lipid vesicles. *Biophys. J.* 64:642–653.
9. Brockman, H. 1994. Dipole potential of lipid membranes. *Chem. Phys. Lipids.* 73:57–79.
10. McLaughlin, S., and A. Aderem. 1995. The myristoyl-electrostatic switch: a modulator of reversible protein-membrane interactions. *Trends Biochem. Sci.* 20:272–276.
11. Cafiso, D. S. 2005. Structure and interactions of C2 domains at membrane surfaces. *In* Protein-Lipid Interactions: From Membrane Domains to Cellular Networks. L. K. Tamm, editor. Wiley-VCH, Weinheim, Germany. 444.
12. Killian, J. A. 1998. Hydrophobic mismatch between proteins and lipids in membranes. *Biochim. Biophys. Acta.* 1376:401–415.
13. Piknova, B., E. Perochon, and J. F. Tocanne. 1993. Hydrophobic mismatch and long-range protein/lipid interactions in bacteriorhodopsin/phosphatidylcholine vesicles. *Eur. J. Biochem.* 218:385–396.
14. Dumas, F., M. C. Lebrun, and J. F. Tocanne. 1999. Is the protein/lipid hydrophobic matching principle relevant to membrane organization and functions? *FEBS Lett.* 458:271–277.

15. Lee, A. G. 1998. How lipids interact with an intrinsic membrane protein: the case of the calcium pump. *Biochim. Biophys. Acta.* 1376: 381–390.

16. Lee, A. G. 2004. How lipids affect the activities of integral membrane proteins. *Biochim. Biophys. Acta.* 1666:62–87.

17. Cornea, R. L., and D. D. Thomas. 1994. Effects of membrane thickness on the molecular dynamics and enzymatic activity of reconstituted Ca-ATPase. *Biochemistry.* 33:2912–2920.

18. Webb, R. J., J. M. East, R. P. Sharma, and A. G. Lee. 1998. Hydrophobic mismatch and the incorporation of peptides into lipid bilayers: a possible mechanism for retention in the Golgi. *Biochemistry.* 37:673–679.

19. Hong, H., and L. K. Tamm. 2004. Elastic coupling of integral membrane protein stability to lipid bilayer forces. *Proc. Natl. Acad. Sci. USA.* 101:4065–4070.

20. Lewis, B. A., and D. M. Engelman. 1983. Bacteriorhodopsin remains dispersed in fluid phospholipid bilayers over a wide range of bilayer thicknesses. *J. Mol. Biol.* 166:203–210.

21. Weiss, T. M., P. C. van der Wel, J. A. Killian, R. E. Koeppe 2nd, and H. W. Huang. 2003. Hydrophobic mismatch between helices and lipid bilayers. *Biophys. J.* 84:379–385.

22. Perozo, E. 2006. Gating prokaryotic mechanosensitive channels. *Nat. Rev. Mol. Cell Biol.* 7:109–119.

23. O'Keeffe, A. H., J. M. East, and A. G. Lee. 2000. Selectivity in lipid binding to the bacterial outer membrane protein OmpF. *Biophys. J.* 79:2066–2074.

24. Chimento, D. P., A. K. Mohanty, R. J. Kadner, and M. C. Wiener. 2003. Substrate-induced transmembrane signaling in the cobalamin transporter BtuB. *Nat. Struct. Biol.* 10:394–401.

25. Hubbell, W. L., D. S. Cafiso, and C. A. Altenbach. 2000. Identifying conformational changes with site-directed spin labeling. *Nat. Struct. Biol.* 7:735–739.

26. Hubbell, W. L., A. Gross, R. Langen, and M. A. Lietzow. 1998. Recent advances in site-directed spin labeling of proteins. *Curr. Opin. Struct. Biol.* 8:649–656.

27. Fanucci, G. E., and D. S. Cafiso. 2006. Recent advances and applications of site-directed spin labeling. *Curr. Opin. Struct. Biol.* 16:644–653.

28. Fanucci, G. E., K. A. Coggshall, N. Cadieux, M. Kim, R. J. Kadner, and D. S. Cafiso. 2003. Substrate-Induced conformational changes of the perplasmic N-terminus of an outer-membrane transporter by site-directed spin labeling. *Biochemistry.* 42:1391–1400.

29. Columbus, L., T. Kalai, J. Jeko, K. Hideg, and W. L. Hubbell. 2001. Molecular motion of spin labeled side chains in α-helices: analysis by variation of side chain structure. *Biochemistry.* 40:3828–3846.

30. Columbus, L., and W. L. Hubbell. 2002. A new spin on protein dynamics. *Trends Biochem. Sci.* 27:288–295.

31. Columbus, L., and W. L. Hubbell. 2004. Mapping backbone dynamics in solution with site-directed spin labeling: GCN4–58 bZip free and bound to DNA. *Biochemistry.* 43:7273–7287.

32. Slichter, C. P. 1978. Principles of Magnetic Resonance. Springer-Verlag, New York.

33. Fanucci, G. E., N. Cadieux, C. A. Piedmont, R. J. Kadner, and D. S. Cafiso. 2002. Structure and dynamics of the β-barrel of the membrane transporter BtuB by site-directed spin labeling. *Biochemistry.* 41: 11543–11551.

34. Lewis, B. A., and D. M. Engelman. 1983. Lipid bilayer thickness varies linearly with acyl chain length in fluid phosphatidylcholine vesicles. *J. Mol. Biol.* 166:211–217.

35. Kucerka, N., S. Tristram-Nagle, and J. F. Nagle. 2005. Structure of fully hydrated fluid phase lipid bilayers with monounsaturated chains. *J. Membr. Biol.* 208:193–202.

36. Lietzow, M. A., and W. L. Hubbell. 2004. Motion of spin label side chains in cellular retinol-binding protein: correlation with structure and nearest-neighbor interactions in an antiparallel beta-sheet. *Biochemistry.* 43:3137–3151.

37. Guo, Z., D. Cascio, K. Hideg, T. Kalai, and W. L. Hubbell. 2007. Structural determinants of nitroxide motion in spin-labeled proteins: tertiary contact and solvent-inaccessible sites in helix G of T4 lysozyme. *Protein Sci.* 16:1069–1086.

38. Mchaourab, H., M. Lietzow, K. Hideg, and W. Hubbell. 1996. Motion of spin-labeled side-chains in T4 lysozyme. (I) Correlation with protein structure and dyanmics. *Biochemistry.* 35:7692–7704.

39. Bloom, M., E. Evans, and O. G. Mouritsen. 1991. Physical properties of the fluid lipid-bilayer component of cell membranes: a perspective. *Q. Rev. Biophys.* 24:293–397.

40. Cadieux, N., P. G. Phan, D. S. Cafiso, and R. J. Kadner. 2003. Differential substrate-induced signaling through the TonB-dependent transporter BtuB. *Proc. Natl. Acad. Sci. USA.* 100:10688–10693.

41. Park, S. H., and S. J. Opella. 2005. Tilt angle of a trans-membrane helix is determined by hydrophobic mismatch. *J. Mol. Biol.* 350:310–318.

42. Stopar, D., J. Strancar, R. B. Spruijt, and M. A. Hemminga. 2006. Motional restrictions of membrane proteins: a site-directed spin labeling study. *Biophys. J.* 91:3341–3348.

43. Farahbakhsh, Z. T., C. Altenbach, and W. L. Hubbell. 1992. Spin-labeled cysteines as sensors for protein-lipid interaction and conformation in rhodopsin. *Photochem. Photobiol.* 56:1019–1033.

44. Perozo, E., and D. C. Rees. 2003. Structure and mechanism in prokaryotic mechanosensitive channels. *Curr. Opin. Struct. Biol.* 13:432–442.

45. Nielsen, C., M. Goulian, and O. S. Andersen. 1998. Energetics of inclusion-induced bilayer deformations. *Biophys. J.* 74:1966–1983.

46. Yau, W. M., W. C. Wimley, K. Gawrisch, and S. H. White. 1998. The preference of tryptophan for membrane interfaces. *Biochemistry.* 37: 14713–14718.

47. Tamm, L. K., A. Arora, and J. H. Kleinschmidt. 2001. Structure and assembly of beta-barrel membrane proteins. *J. Biol. Chem.* 276:32399–32402.

48. Faraldo-Gomez, J. D., G. R. Smith, and M. S. P. Sansom. 2003. Molecular dynamics simulations of the bacterial outer membrane protein FhuA: a comparative study of the ferrichrome-free and bound states. *Biophys. J.* 85:1406–1420.

49. Coggshall, K. A., N. Cadieux, C. Piedmont, R. Kadner, and D. S. Cafiso. 2001. Transport-defective mutations alter the conformation of the energy-coupling motif of an outer membrane transporter. *Biochemistry.* 40:13946–13971.

50. Gumbart, J., M. C. Wiener, and E. Tajkhorshid. 2007. Mechanics of force propagation in TonB-dependent outer membrane transport. *Biophys. J.* 93:496–504.

51. Postle, K., and R. Kadner. 2003. Touch and go: tying TonB to transport. *Mol. Microbiol.* 49:869–882.